Composites Part B 224 (2021) 109168

Contents lists available at ScienceDirect

Composites Part B

journal homepage: www.elsevier.com/locate/compositesb

Three-dimensional skeleton assembled by carbon nanotubes/boron nitride as filler in epoxy for thermal management materials with high thermal conductivity and electrical insulation

Wang Yang [1], Yifan Wang [1], Yun Li, Can Gao, Xiaojuan Tian, Ni Wu, Zishuo Geng, Sai Che, Fan Yang, Yongfeng Li [*]

State Key Laboratory of Heavy Oil Processing, China University of Petroleum, Beijing, Changping, 102249, PR China

ARTICLE INFO

Keywords:
Boron nitride
Carbon nanotubes
Three-dimensional structure
Thermal conductivity
Thermal management materials

ABSTRACT

Due to high aspect ratio, excellent thermal conductivity, and electrical insulation, boron nitride exhibits a great potential in the field of electronic packaging. However, its longitudinal thermal conductivity is far poor than horizontal thermal conductivity, which limits its application in a wider field. Herein, a three-dimensional (3D) network structure is constructed by coating boron nitride nanosheets/carbon nanotubes on foam skeleton derived from the commercial polyurethane (PU) (3D BNNS/CNTs). The *in-situ* grown CNTs on the surface of BNNS produce an interconnected network structure. The resultant 3D skeleton coupled with cross-linked BNNS/CNTs endows it with excellent thermal and mechanical properties. After curing with epoxy resin, the optimized 3D BNNS/CNTs$_{15\ \%}$/Epoxy composite obtains a high thermal conductivity of 1.49 W m^{-1} K^{-1} at a low loading of 20 wt%, which achieves a thermal conductivity enhancement of 1046 % compared to neat epoxy resin. Meanwhile, the synthesized 3D BNNS/CNTs$_{15\ \%}$/Epoxy composite maintains a high electrical resistivity above 10^{10} Ω m, high elastic modulus of 1.0 GPa and tensile stress of 35 MPa. Thus, this strategy may offer a new insight for constructing advanced packaging materials with excellent thermal and mechanical performances for electronic device.

1. Introduction

The rapid development of the fifth generation mobile communication technology puts forward higher requirements for the heat dissipation of electronic devices. Therefore, it is necessary for developing an excellent heat dissipation material for ensuring the long life of equipment [1–3]. Ideal thermal management materials (TMMs) for electronic equipment should be characterized by high thermal conductivity, excellent electrical insulation, good thermal and mechanical stability, and low cost [4–8]. Traditional TMMs, such as epoxy and polyethylene, have good thermoplasticity, but their thermal conductivity is relatively lower. Recently, some novel nanomaterials, such as graphene [9], boron nitride nanosheets (BNNS) [10–12], and carbon nanotubes (CNTs) [13], have attracted great attention due to their superior thermal conductivity and mechanical strength, but their plasticity are relatively poor.

Different from conductive carbon materials, BNNS are identified as an intriguing candidate filler for the electrical insulating TMMs, which can avoid short circuit of the electronic devices [14–16]. However, compared with carbon-based TMMs, the thermal conductivity of BNNS is relatively low, which limits its application. Common strategies to improve thermal performance of BNNS include functionalization [17, 18] and construction of three dimensional (3D) self-assembled structure [19]. The former can usually enhance the interface interaction between the filler and matrix, leading to strong bonding and adhesion [20], but it often obtains a smaller thermal enhancement. Meanwhile, accompanied by the use of large amounts of organic solvents, which is harmful for environment. By contrast, constructing 3D network structure becomes the attractive choice, which can achieve higher thermal enhancement derived from the interconnected structure [21]. For example, Zhou et al. prepared a 3D BNNS/cross-linked polystyrene composite by using purified water as a foaming agent. Benefiting from its 3D structure, it obtained a high thermal conductivity of 1.28 W m^{-1} K^{-1} [22]. In addition, Liu et al. fabricated a 3D polystyrene/polypropylene/BN ternary composite by solution-mixing and hot-pressing method. The densely

* Corresponding author.
E-mail addresses: wyang@cup.edu.cn (W. Yang), yfli@cup.edu.cn (Y. Li).
[1] The first two authors contributed equally to this work.

https://doi.org/10.1016/j.compositesb.2021.109168
Received 3 June 2021; Received in revised form 13 July 2021; Accepted 21 July 2021
Available online 23 July 2021

interconnected 3D segregated filler networks endowed it the thermal conductivity of 5.57 W m^{-1} K^{-1} with 50 wt% BN [23]. Nevertheless, these above works can only obtain the impressive thermal conductive enhancement with relatively high filler content, which always cause the high cost. It is still a challenge for preparing a high thermal conductivity composite with low filler content. Beyond that, in order to be suitable for different types of electronic devices, the insulation and mechanical properties of composite materials should be taken into account as well, which will put forward higher requirements for the development of TMMs.

Herein, we fabricate a 3D network structure by anchoring BNNS/carbon nanotubes on foam skeleton (3D BNNS/CNTs) with the assistance of self-sacrificial polyurethane template. Compared with other methods such as ice template or CVD method, the foam template method is simple, easy to expand and can be mass-produced, which is more attractive due to its ability to produce clear-shaped structures. The in-situ grown long and tangled CNTs act as a bridge between BNNS and entangle them, and fully contacted BNNS and CNTs ensure excellent mechanical property. Meanwhile, the cross-linking between CNTs and BNNS forms a three-dimensional thermally conductive filler, which not only greatly improves the connectivity between BNNS, but also makes a strong interface bonding force between CNTs and BNNS. The resultant 3D BNNS/CNTs are encapsulated by epoxy resin to obtain the 3D BNNS/CNTs/Epoxy composites. When served as the TMMs, it reaches a high thermal conductivity of 1.49 W m^{-1} K^{-1} at a filler of 20 wt%. More importantly, it still maintains an excellent electrical insulation and gains high elastic modulus (1.0 GPa) and tensile stress (35 MPa). These results demonstrate that this developed 3D network composite realizes the high thermal and mechanical performance enhancement at a low filler loading. This may provide a new insight into the preparation of polymer composites with excellent thermal and mechanical properties for electronic packaging.

2. Experimental section

2.1. Materials

Commercial polyurethane foam (PU) used for kitchen supplies was used in this work. Immersing it in the BNNS/CNTs suspension, due to the porous structure and strong adsorption capacity of the polymer sponge, the BNNS/CNTs is introduced into the sponge and evenly coated on sponge skeleton. Hexagonal boron nitride powder was bought from Liaoning DCEL Co., Ltd, China. Nickel acetate ($Ni(CH_3COO)_2$) was bought from Beijing Huawei Chemical Co., Ltd. Aliphatic Epoxy resin (6105) and hardener of methyl-hexahydrophthalic anhydride (MHHPA) were obtained from DOW Chemicals (USA) and Shanghai Li Yi Science & Technology Development Co. Ltd. (China). Ethylene, hydrogen, and argon were supplied by Beijing AP BAIF Gases Industry Co., Ltd. All chemicals were used as received without further purification.

2.2. Preparation of BNNS/CNTs composites materials

In this work, BNNS were first obtained by supercritical CO_2 exfoliation method according to our previously developed work [24]. For the synthesis of BNNS/CNTs, a certain amount of BNNS and nickel acetate were dispersed in isopropyl alcohol. The mixture was ultrasonicated for 6 h, followed by stirring magnetically overnight. Next, the mixture was evaporated by rotary evaporator at 60 °C to obtain the Ni salts/BNNS precursors. Then, the as-prepared precursors were placed in fluidized bed reactor, and reacted at 500 °C under mixed Ar/H_2 at a flow rate of 300/30 sccm for 10 min to obtain Ni@BNNS mixture. Next, continue to heat up to 660 °C, until the temperature stabilizes, the ethylene was introduced as the carbon source at a flow rate of 30 sccm. The growth time of CNTs was controlled from 5 to 15 min, and the resultant BNNS/CNTs was collected until the temperature was cooled to room temperature.

2.3. Preparation of 3D BNNS/CNTs/Epoxy composites

BNNS/CNTs were evenly dispersed in ethanol through an ultrasonic and stirring treatment. Then, PU was submerged in above suspension with ultrasonic treatment for 4 h. After centrifugation and drying processes, the surfaces of PU foam skeleton were covered with the BNNS/CNTs, forming BNNS/CNTs/PU composites. Eventually, the PU in BNNS/CNTs/PU composite was pyrolyzed at 380 °C under Ar atmosphere for 1 h, thereby obtaining 3D BNNS/CNTs composites.

The 3D BNNS/CNTs/Epoxy composites were prepared via the solution blending methods. The epoxy resin was placed in a vacuum oven for 30 min to remove the bubbles, and then poured into the 3D BNNS/CNTs composite, followed by transferred into an oven to cure at 165 °C for 12 h. Finally, the 3D BNNS/CNTs/Epoxy composite was obtained. More detailed method for achieving different filler loading in the epoxy matrix is provided in the Supporting Information. For comparisons, 3D BNNS/Epoxy composite was fabricated under the same condition but without CNTs. Likewise, BNNS/CNTs/Epoxy and BNNS/Epoxy composites were also developed under same condition but without the PU treatment process.

2.4. Characterizations

The morphology and microstructure of samples were examined by using scanning electron microscopy (SEM, Hitachi SU8010), transmission electron microscope (TEM, FEI, Tecnai G2 F20) and atomic force microscopy (AFM, Bruker Multimode 8). The CNTs mass fraction of BNNS/CNTs samples was carried out using a thermogravimetric analysis (TGA, Netzsch, STA7200, Germany) from 30 to 800 °C at a ramp rate of 10 °C min^{-1} under air atmosphere. The structure were conducted on Xplora plus Raman microscope system (Horiba scientific) using a laser with an excitation wavelength of 532 nm, and the crystalline structure was examined by X-ray diffractometer (XRD) on a Bruker D8 ADVANCE using Cu Kα radiation ($\lambda = 1.5418$ Å). The thermal conductivity of composites was tested on a TIM Thermal Resistance & Conductivity Measurement Apparatus (LW-9389, Long Win Science & Technology Co). The surface temperature distribution photos of the composites and LED chips were captured by an infrared thermal camera (FLIR E50). The electrical properties of composites were measured by a high voltage insulation tester (TA8322A), and the mechanical properties of obtained composites were obtained by Zwick Roell Z010 testing machine according to the DIN ISO 34-1 standard. The thermal expansion coefficient of composites was tested by a high temperature thermal dilatometer from Waters Corporation of the United States, and the viscosity of nanofluid was measured using the Physica MCR 301 R rheometer. More detailed procedure about the thermal conductivity and electrical resistivity test methods have been provided in Supporting Information.

3. Results and discussion

3.1. Morphology structure of BNNS, BNNS/CNTs, 3D BNNS, and 3D BNNS/CNTs

The schematic illustration of the 3D BNNS/CNTs composite has been presented in Fig. 1. Briefly, BNNS/CNTs are first produced through in-situ growth of CNTs on the surfaces of BNNS with the catalysis effect of Ni. Here, the introduced CNTs can act as a bridge between the BNNS, forming an interconnected network structure. Then, 3D BNNS/CNTs structure is successfully constructed with using PU foam as a self-sacrificing template and BNNS/CNTs as building blocks. The morphology and microstructure of composites are investigated by SEM. It is clearly seen that pristine BNNS exhibit a thin nanosheet structure (Fig. 2a), which is similar to graphene, confirming the availability of supercritical CO_2 exfoliation strategy. Moreover, the height and length of BNNS can be charactered by AFM (Figure S1). It can be seen that the

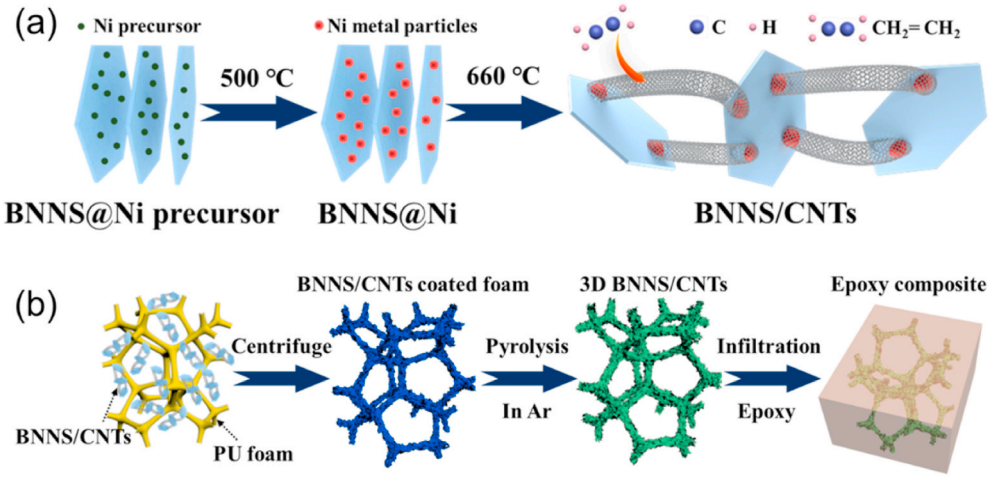

Fig. 1. (a) Schematic illustration of the fluidized bed chemical vapor deposition process for the fabrication of BNNS/CNTs. (b) Schematic illustration of the formation process of 3D BNNS/CNTs/Epoxy composie.

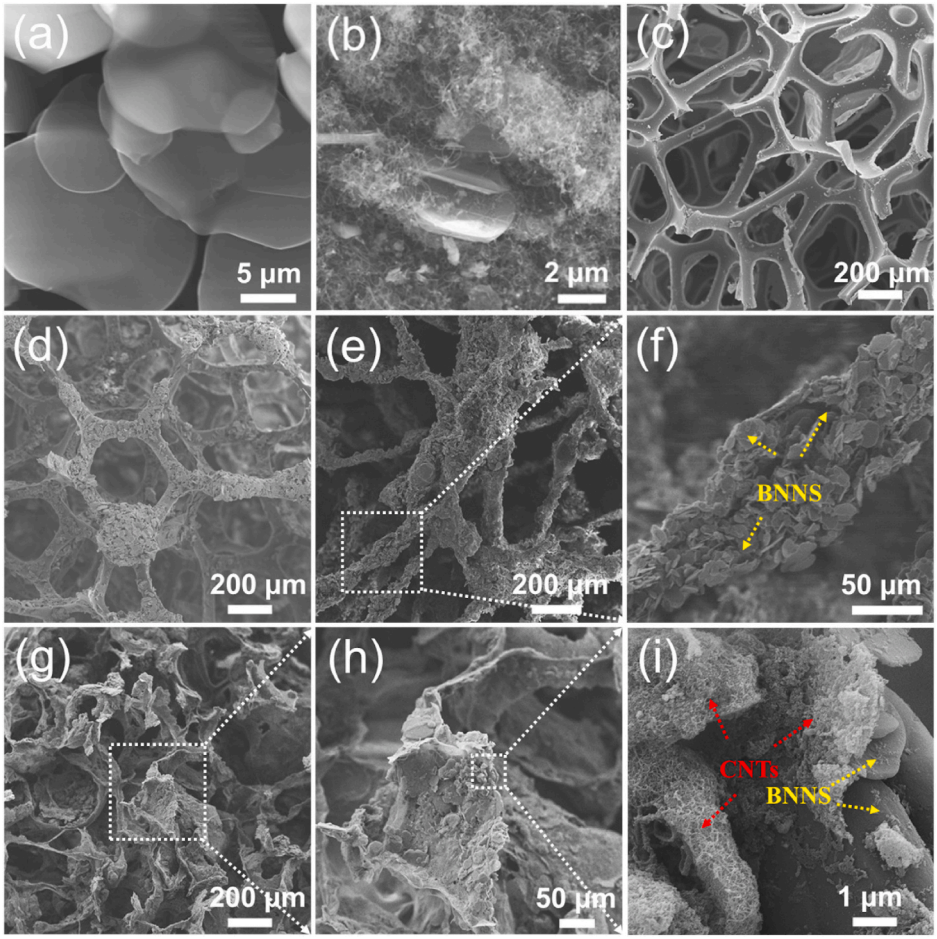

Fig. 2. SEM image of (a) BNNS prepared by supercritical CO_2 exfoliation technology, (b) BNNS/$CNTs_{15\ \%}$ prepared by Fluidized bed chemical vapor deposition, (c) the pristine PU foam, (d) BNNS coated on the surface of PU, (e–f) 3D BNNS, and (g–h) 3D BNNS/$CNTs_{15\ \%}$ samples, (i) Enlarged image of BNNS/$CNTs_{15\ \%}$.

height of BNNS is about 1.75 nm and the length is about 600 nm.

The SEM images of BNNS/Ni salt and BNNS/Ni are shown in Figure S2a-d. After the high temperature reduction in H_2 atmosphere, metallic Ni is distributed on the surfaces of BNNS and acted as catalysts for the growth of CNTs. In addition, the element mapping results (Figure S2e-h) also confirm the distribution of B, N and Ni, which further proves the successful synthesis of BNNS/Ni. For BNNS/CNTs sample, the density of CNTs on BNNS substrates can be well controlled via regulating the deposition time of carbon atoms. It is found that the amount of CNTs gradually increases with the increasing of growth time. The content of CNTs can be obtained from the thermogravimetric curves (Figure S3). The results show that the CNTs contents of several BNNS/CNTs samples

reach 6 %, 15 % and 23 % when the growth time is 5, 10 and 15 min, respectively. Thereby, these obtained samples are denoted as BNNS/CNTs$_x$, where x is the mass fraction of CNTs in the composites. Indeed, the SEM images of BNNS/CNTs$_{6\%}$ exhibits relatively short and sparse CNTs (Figure S4a). With further increase of growth time, the density of CNTs becomes denser, which interconnects between the BNNS and forming a cross-linked network structure (Fig. 2b and Figure S4b-d). It can be seen from the TEM images that the carbon material is in the form of multi-walled carbon nanotubes (Figure S4e-f).

The pristine PU foam with a big average cellular size of ~300 μm (Fig. 2c) is used as a template for generating a 3D interconnected structure, which can guarantee that the epoxy composites obtain excellent mechanical performance at relatively low fillers loading. Furthermore, BNNS and BNNS/CNTs are used as building blocks to tightly anchor on the skeleton of PU foam, producing complete thermal conduction pathways. Fig. 2d displays that the BNNS evenly covers on the surfaces of foam skeleton for BNNS/PU sample. After calcination treatment, the 3D BNNS samples can still maintain the cellular structure of the PU frameworks, and BNNS are still covered on the whole skeleton surfaces (Fig. 2e and f). Interlinked BNNS build an ideal thermal conductive channel, which thus can improve the thermal conductivity of the composites. More importantly, the 3D BNNS/CNTs composite also retains the 3D skeleton structure after calcination process (Fig. 2g and h), and its macroscopic size have no significant change (Figure S5a). Next, a TGA test is performed on the 3D BNNS/CNTs$_{15\ \%}$/Epoxy with different filler loadings. As displayed in Figure S5b, the calculated values of content are about 5 %, 10 %, 15 %, and 20 wt% respectively, which is consistent with the addition amount. Meanwhile, the BNNS/CNTs contact and well stack one by one along the skeleton to form a continuous network (Fig. 2i), which promote the thermal and mechanical properties of resultant composites.

To investigate the crystalline structure of samples, XRD is conducted. As shown in Fig. 3a, the diffraction peaks of four samples correspond to (002), (100), (101), (102), and (004) planes [25], with lattice constants of a = 0.25 nm and c = 0.666 nm (JCPDS Card No. 34–0421) [26], proving the presence of BN phase. It is worth noting that the XRD characteristic peaks of CNTs overlap with the position of BNNS (002) crystal plane to a certain extent, so the characteristic peaks are covered. Meanwhile, it can be seen that the (002) peak is significantly stronger than other diffraction peaks, which should be attributed to the exposure of (002) crystal plane. Figure S6a displays that the main peak of (002) plane occurs a shift, indicating the successful combination of CNTs and BNNS. In addition, two new peaks appear at 44.4° and 51.8° from the XRD spectra of BNNS/Ni and BNNS/CNTs (Figure S6b), suggesting the existence of Ni (JCPDS Card No. 04–0850) [27]. This result proves that the Ni precursor has been reduced to metal Ni, which then serves as a catalyst for the growth of CNTs. Raman spectra are performed to further characterize the compositions of BNNS/CNTs, and BNNS, as exhibited in Fig. 3b. Actually, the Raman peak of the BNNS occurs at 1368 cm^{-1}, owing to the vibrational mode (E_{2g}) of BNNS materials [24]. Interestingly, after combining with CNTs, the BNNS/CNTs shows two strong peaks at about 1346 and 1576 cm^{-1} [28]. The peak near 1576 cm^{-1} corresponds to G peak of carbon, and the peak near 1346 cm^{-1} should be attributed to the D peak of carbon and E_{2g} bond vibration peak of BN [29]. Owing to the similarity and coincidence of the Raman characteristic peaks of BN and CNTs, the split-peak fitting is performed (Fig. 3b). The result shows that the Raman peak is indeed consisted of a wide D peak of CNTs and high E_{2g} peak of BNNS, indicating a good combination of BNNS and CNTs [30].

3.2. Thermal properties of 3D BNNS/CNTs/Epoxy

In order to measure the thermal performances, the samples are blended together with epoxy to prepare epoxy composites. As shown in Figure S7a-d, the SEM images of 3D BNNS/Epoxy, and 3D BNNS/CNTs$_{15\ \%}$/Epoxy composites with filler loading of 10, 15 and 20 wt%

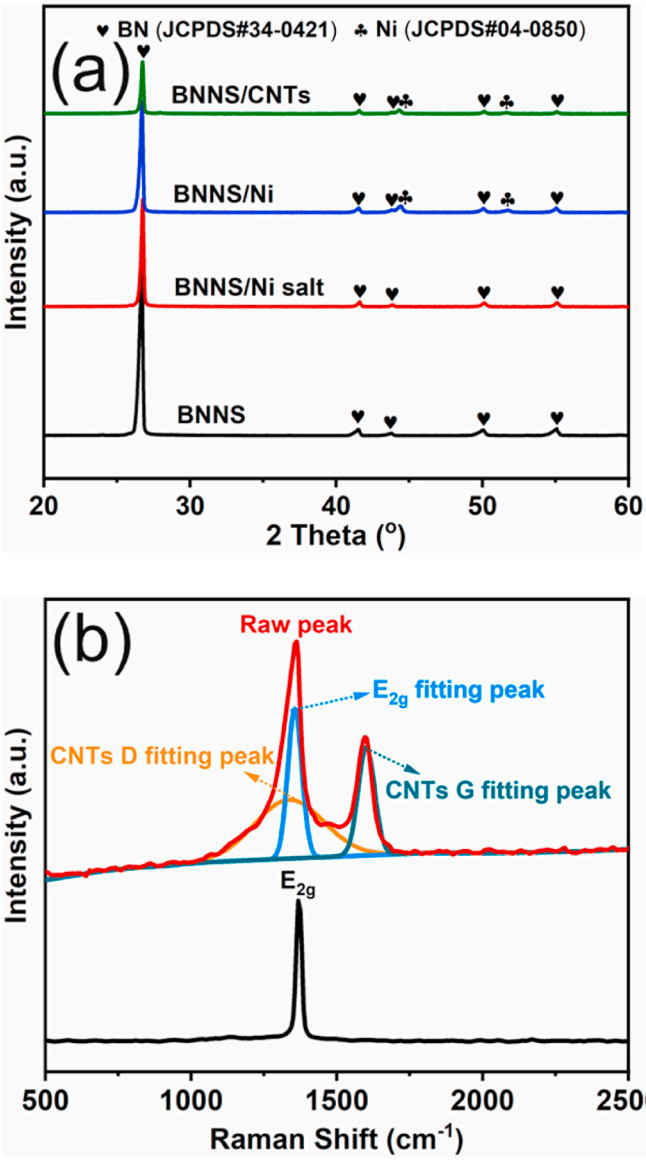

Fig. 3. (a) XRD patterns of BNNS, BNNS/Ni salt, BNNS/Ni, and BNNS/CNTs. (b) Raman spectra of BNNS and BNNS/CNTs, and corresponding fitted peaks.

clearly indicate that the interconnected 3D network is well maintained throughout the epoxy matrix. The thermally conductive filler is well encapsulated by epoxy matrix with excellent interface bonding between the filler and matrix, and no obvious pore is observed. These are the key factors for the decrease of interface thermal resistance between the filler and epoxy resin [31,32]. Benefiting from the unique 3D thermal network structure, 3D BNNS/Epoxy composite reaches a higher thermal conductivity of 1.25 W m^{-1} K^{-1} than that of BNNS/Epoxy (0.93 W m^{-1} K^{-1}) at a filler content of 20 wt%. Likewise, the 3D BNNS/CNTs/Epoxy composite delivers a much higher thermal conductivity (1.49 W m^{-1} K^{-1}) than that of BNNS/CNTs/Epoxy (1.13 W m^{-1} K^{-1}), confirming the superiority of constructed 3D structure (Fig. 4a). Impressively, the CNTs exert a vital role in enhancing the heat-conducting capability. As exhibited in Fig. 4b, after the introduction of CNTs specie, the epoxy composites obtain a better thermal performance due to the thermal bridge formed by CNTs. Moreover, as the introduction of CNTs increases, the thermal conductivities of 3D BNNS/CNTs/Epoxy composites gradually increase. The thermal conductivities of 3D BNNS/CNTs$_{6\%}$/Epoxy, 3D BNNS/CNTs$_{15\%}$/Epoxy, and 3D BNNS/CNTs$_{23\ \%}$/Epoxy can reach 1.01, 1.49, and 1.74 W m^{-1} K^{-1} at a filler content of 20 wt%,

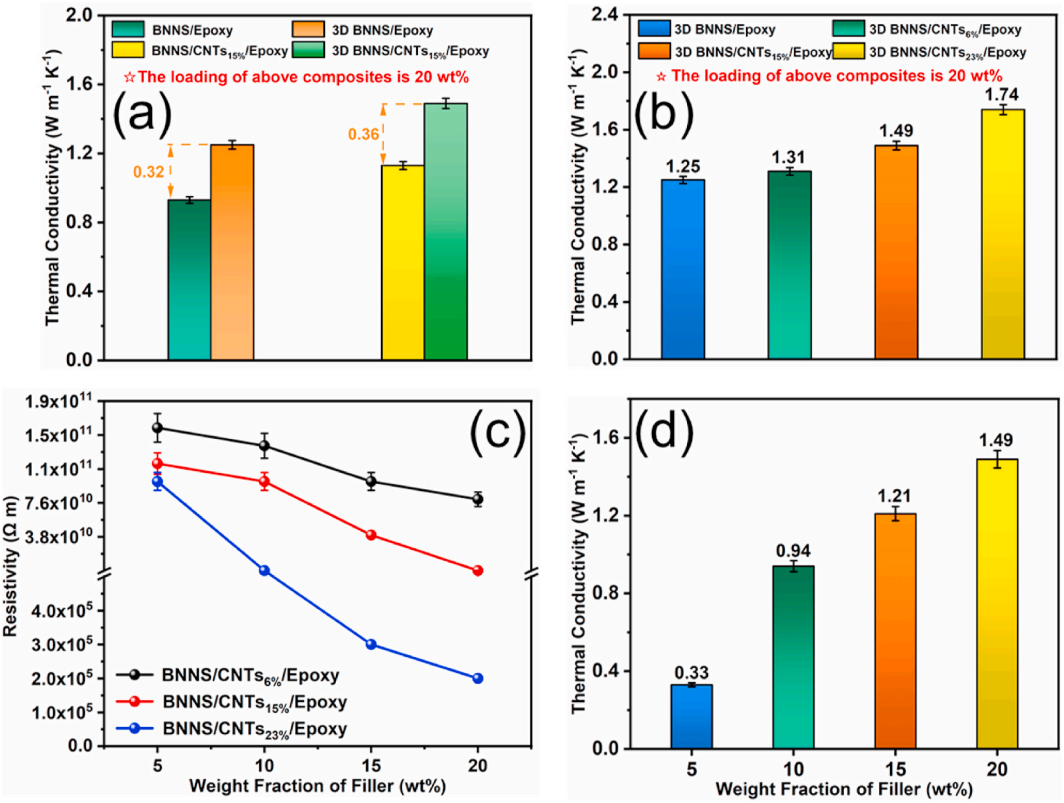

Fig. 4. (a) The enhancement of 3D network structure on thermal conductivity. (b) Thermal conductivity of 3D BNNS/CNTs$_x$/Epoxy composites with different CNTs content. (c) Electrical conductivity of epoxy composites with the different BNNS/CNTsx loading (x = 6, 15, 23 %). (d) Thermal conductivity of 3D BNNS/CNTs15 %/Epoxy composite with different filler loading.

respectively. Moreover, the BNNS/CNTs/Epoxy composites with randomly distributed BNNS/CNTs were also prepared by directly adding BNNS/CNTs into the epoxy resin at same curing procedure, and the thermal conductivity of the composites with a filler loading of 20 wt% were tested (Figure S7e).

It is known that BNNS possess a fascinating feature in electrical insulating heat conduction materials. However, the incorporation of CNTs would affect this character. The resistances of resultant epoxy composites gradually decrease with increasing the introduction of CNTs (Fig. 4c). Interestingly, when the content of CNTs is 6 % and 15 %, the epoxy composites still maintain high electrical resistivities above 10^{10} Ω m at the filler loading of 5, 10, 15, and 20 wt%, suggesting an electrical insulation. With a further increase of CNTs, the resistivity of the 3D BNNS/CNTs$_{23\ \%}$/Epoxy composite decreases to be a conductor, which should be attributed to the conductive pathways connected by the dense CNTs in abundant amount. That is to say, 3D BNNS/CNTs$_{15\ \%}$/Epoxy composite obtains not only a good thermal conductivity, but also can maintain a good electrical insulation to guarantee the merits of boron nitride materials. Such composite material exhibits a great promising to avoid short circuit of electronic devices. Therefore, we choose 3D BNNS/CNTs$_{15\ \%}$/Epoxy as the optimized sample to further conduct the follow-up studies.

Fig. 4d shows the influence of amount of filler in 3D BNNS/CNTs$_{15\ \%}$/Epoxy composites. It can be seen that when the filler loading content of 3D BNNS/CNTs$_{15\ \%}$ is smaller, the composite can only obtain a low thermal conductivity. This is attributed that the composite cannot reach the thermal percolation threshold at a lower loading fraction [33], under which the thermal conductivity of the epoxy composite shows a relatively slow increasing trend. However, with further increase the addition of filler to 20 wt%, the 3D BNNS/CNTs$_{15\ \%}$/Epoxy composite reach the thermal percolation threshold, and it can achieves a high thermal conductivity of 1.49 W m^{-1} K^{-1}, which is much better than those of other epoxy counterparts. This encouraged thermal ability should be attributed to the construction of efficient phonon transport path produced by the 3D BNNS/CNTs$_{15\ \%}$ component. Moreover, Figure S7f shows the effect of filler loading on thermal conductivity in other epoxy composites prepared in this work.

To further verify and contrast the enhanced thermal dissipation performance, the temperature distribution of 3D BNNS/CNTs$_{15\ \%}$/Epoxy, BNNS/CNTs$_{15\ \%}$/Epoxy, and pure epoxy resin with cooling time is measured by an infrared thermal camera. Firstly, the samples are placed in an oven for 10 min at 130 °C to obtain a uniform surface temperature. After transferring to room temperature, the surface temperature of epoxy composites is detected in real time. As shown in Fig. 5a, the surface temperature of 3D BNNS/CNTs$_{15\ \%}$/Epoxy decreases more faster with cooling time than those of pure epoxy resin and BNNS/CNTs$_{15\ \%}$/Epoxy, which can be attributed to the high thermal conductivity of 3D BNNS/CNTs$_{15\ \%}$/Epoxy. In terms of the test data, the temperature drop trend of 3D BNNS/CNTs$_{15\ \%}$/Epoxy is obviously faster than those of pure epoxy resin and BNNS/CNTs$_{15\ \%}$/Epoxy. The specific values are shown in Fig. 5b. When the cooling time is 1 min, the temperature of 3D BNNS/CNTs$_{15\ \%}$/Epoxy is close to 57.3 °C, which is obviously lower than that of the BNNS/CNTs$_{15\ \%}$/Epoxy (77.9 °C). Furthermore, the BNNS/CNTs$_{15\ \%}$/Epoxy can take 73 s to cool to 70 °C, while the 3D BNNS/CNTs$_{15\ \%}$/Epoxy only takes 39 s. The 34 s difference shows the superiority of the 3D BNNS/CNTs$_{15\ \%}$/Epoxy as TMMs due to its excellent heat dissipation ability. More encouragingly, as depicted in Fig. 5c, the 3D BNNS/CNTs$_{15\ \%}$/Epoxy composite prepared in this work performs a much better thermal performance in comparison with previously reported works on the polymeric composites filled with boron nitride and its derivatives [34–48]. Further information is provided in Table S1.

Such excellent thermal and electrical properties make 3D BNNS/CNTs$_{15\%}$/Epoxy as an attractive candidate for TMMs. To verify this

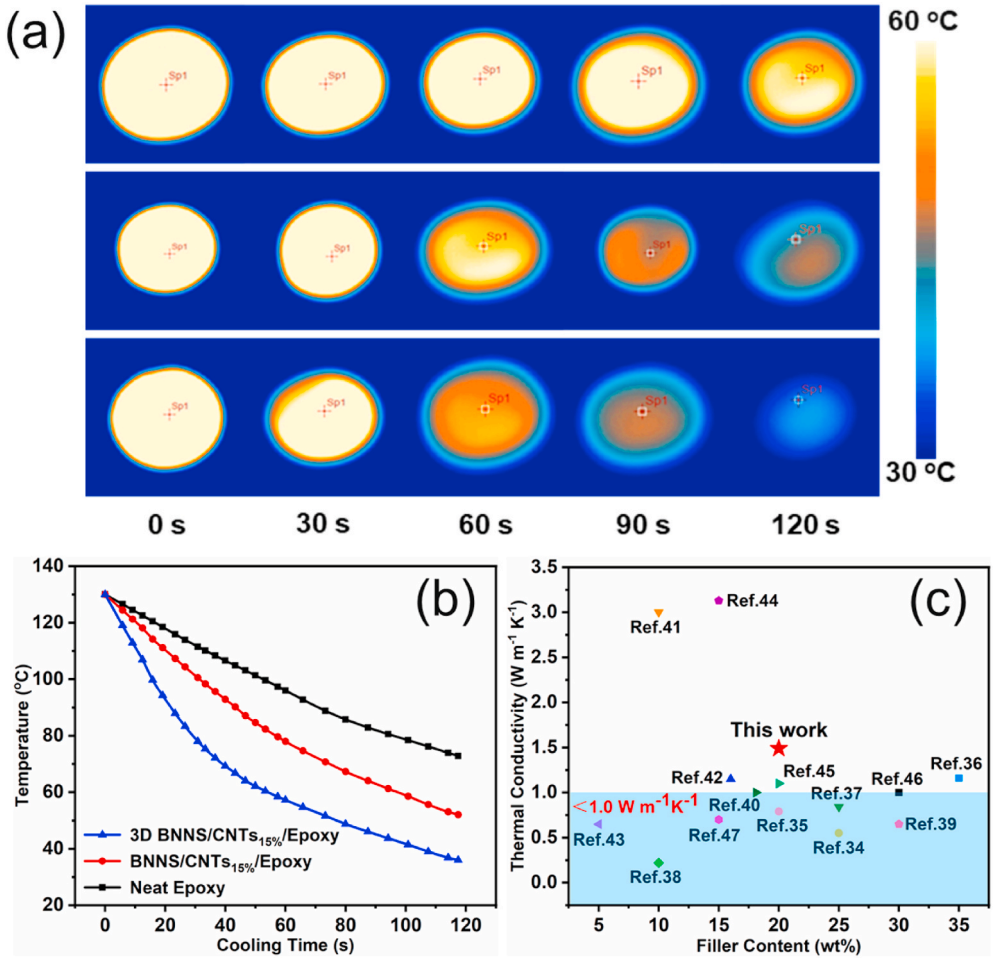

Fig. 5. (a) Infrared thermal images of neat epoxy , 3D BNNS/Epoxy composite and 3D BNNS/CNTs$_{15\ \%}$/Epoxy composite. (b) Temperature-time curve measured at the center of samples surface of neat epoxy, 3D BNNS/Epoxy composite and 3D BNNS/CNTs$_{15\ \%}$/Epoxy composite. (c) Comparison of the thermal conductivities for the different epoxy composites.

point, a commercial silicone sheet and 3D BNNS/CNTs$_{15\%}$/Epoxy are successively employed as TMMs in between a 30 W light-emitting device (LED) chip and a Cu heat sink (Fig. 6a and b). The Cu heat sink is used to remove the heat rapidly. However, the interface roughness can causes incomplete surface contact and thermal contact resistance. Typically, the thermal grease is employed to improve bonding between the LED chip/TMMs/Cu heat sink interfaces. In this strategy, the thermal contact resistance can be minimized and heat can dissipate from the LED chip

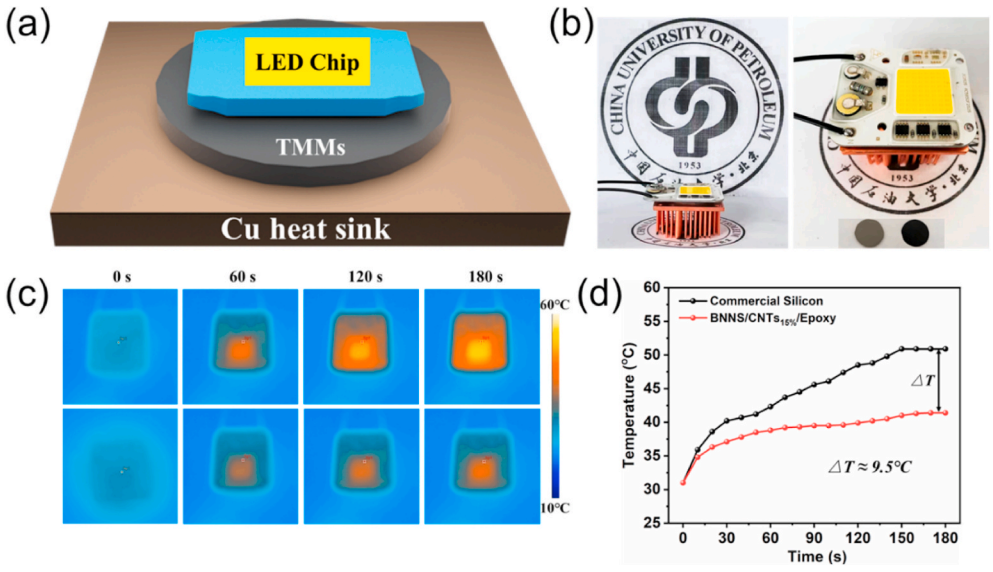

Fig. 6. Demonstration of our 3D BNNS/CNTs$_{15\ \%}$/Epoxy composite as a TMMs. (a) Schematic diagram of LED chip integrated with 3D BNNS/CNTs$_{15\ \%}$/Epoxy composite and a Cu heat sink. (b) Optical photographs of LED chips integrated with commercial silicone sheet and 3D BNNS/CNTs$_{15\ \%}$/Epoxy composite. (c) Infrared thermal images of two LED chips. (d) Comparison the temperature increase of the LED chips when using 3D BNNS/CNTs$_{15\ \%}$/Epoxy composite and commercial silicone sheet, respectively.

fleetingly. After inserting the as-prepared 3D BNNS/CNTs$_{15\%}$/Epoxy between the LED chip and Cu heat sink, the surface temperature is monitored by an infrared camera. As comparison, commercial silicone sheet are tested under the same operating conditions. Fig. 6c exhibits a part of infrared images after turning on the LED chips. With the using of commercial silicone sheet, the surface temperature rises to about 50.9 °C after stabilization. Meanwhile, the 3D BNNS/CNTs$_{15\%}$/Epoxy can stabilize at a relatively lower temperature about 41.4 °C. The increasing trend of surface temperature of LED chip is measured by infrared images (Fig. 6d). It can be distinctly seen that compared to the 3D BNNS/CNTs$_{15\%}$/Epoxy, the commercial silicone sheet displays a much fast increase of temperature. The temperature difference up to 9.5 °C demonstrates that the 3D BNNS/CNTs$_{15\%}$/Epoxy can significantly reduce the heating rate of LED chip than the purchased commercial silicone sheet. In addition, the cycling tests are also performed. It is found that the resultant epoxy composites have good thermal stability during the "on" and "off" cycles process (Figure S8a). Especially considering the low manufacturing cost, it is very economical as TMMs.

Due to the composites based on thermosetting epoxy resin are usually used in the glassy state, the coefficient of thermal expansion (CTE) has been examined. As shown in Figure S8b, the CTE values of composites exhibit a downward trend as the content of filler increased. Specifically, it reaches 143 × 10^{-6} °C^{-1} with a loading of 15 wt%, which is 61.1 % lower than that of neat epoxy resin. Such low value may be attributed to the low CTE of BNNS/CNTs and good interface bonding between the BNNS/CNTs and epoxy resin. To sum up, the developed 3D BNNS/CNTs/Epoxy composites in this work may provide a promising solution for thermal management of high-power electronic equipment in the future.

3.3. Mechanical properties of 3D BNNS/CNTs/Epoxy

Besides thermal conductivity, mechanical property is also an important parameter in the practical applications of TMMs. So we carry out axial tensile test on the epoxy composites. Fig. 7a and **b** show stress-strain curves, tensile stress and elastic modulus of neat epoxy, BNNS/CNTs$_{15\ \%}$/Epoxy and 3D BNNS/CNTs$_{15\ \%}$/Epoxy. The tensile stress of neat epoxy reaches up to 42.0 MPa, which is 1.2 times higher than that of 3D BNNS/CNTs$_{15\ \%}$/Epoxy (35 MPa). In addition, compared with pure epoxy resin, the elastic modulus of 3D BNNS/CNTs$_{15\ \%}$/Epoxy (1.0 GPa) only reduced by 0.4 GPa. It can be seen that the presence of 3D network structure provides a certain degree of supporting force and mechanical strength, resulting in effective transmission of stress along the 3D networks, and has limited impact on the mechanical strength. However, for BNNS/CNTs$_{15\ \%}$/Epoxy with randomly distributed fillers, BNNS/CNTs$_{15\ \%}$ tend to agglomerate in the epoxy matrix through strong van der Waals forces between the layers, and its affinity with epoxy is weak, making it very difficult to uniformly disperse. Therefore, poor dispersion and compatibility make the mechanical properties of BNNS/CNTs$_{15\ \%}$/Epoxy greatly reduced. In short, the existence of 3D network structure not only improves the thermal performance of composites, but also enhances the link between BNNS to hinder the breakage of epoxy composites to greatest extent.

3.4. Rheological properties of 3D BNNS/CNTs/Epoxy fluids

In addition to thermal and mechanical properties, rheological properties are also an important indicator of the TMMs in practical applications. Herein, the viscosity of 3D BNNS/CNTs$_{15\ \%}$ epoxy-based fluids with different filler loading is measured at a shear rate of 20 s^{-1}. As shown in Figure S9a, with the increase of filler loading, the viscosity of epoxy fluids shows an increasing trend, but the increase is limited. This may be attributed to the interaction between the BNNS/CNTs and epoxy resin. It is worth mentioning that although the viscosity of the 3D BNNS/CNTs$_{15\ \%}$ epoxy fluids increases slightly, it is still very close to that of the neat epoxy resin. The photos also present a good fluidity (Figure S9b, c). In fact, when the viscosity of the fluid is large, it will be not conducive for electronic packaging. Therefore, the low viscosity of 3D BNNS/CNTs$_{15\ \%}$ epoxy-based fluid is a prominent advantage in thermal management industry.

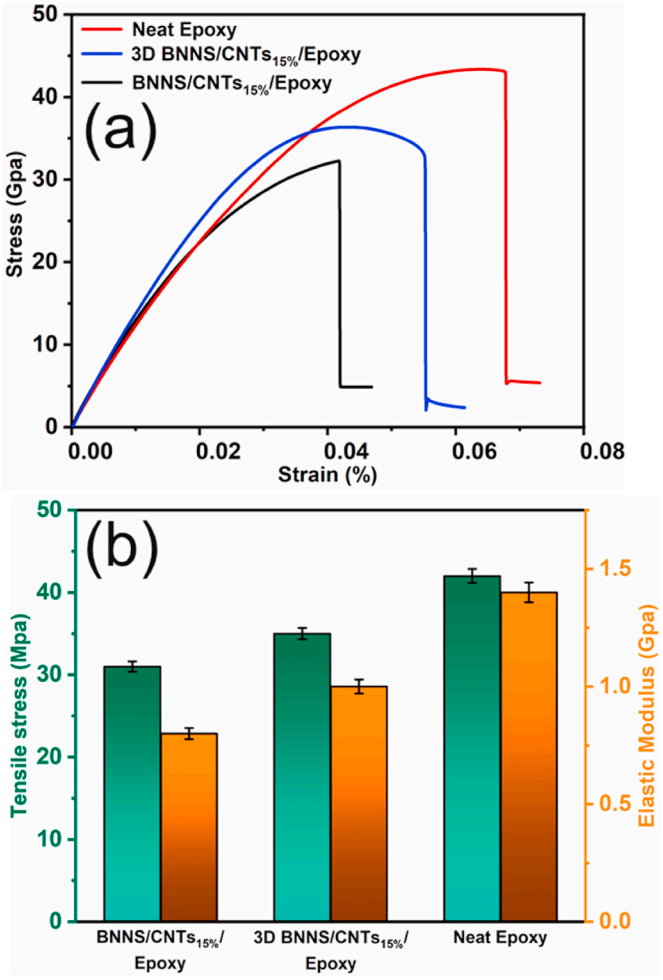

Fig. 7. Mechanical performances of the neat epoxy, BNNS/CNTs$_{15\ \%}$/Epoxy and 3D BNNS/CNTs$_{15\ \%}$/Epoxy. (a) Stress-Strain curves. (b) Elastic modulus and tensile stress.

4. Conclusion

In summary, a 3D network structure is constructed by anchoring BNNS/CNTs on foam skeleton derived from the self-sacrificial templated commercial PU. As a result, a high thermal conductivity of 1.49 W m^{-1} K^{-1} is obtained at a low 3D BNNS/CNTs$_{15\ \%}$ filler of 20 wt%, which corresponds to a thermal conductivity enhancement of about 1046 % compared to the neat epoxy. Impressively, the 3D BNNS/CNTs$_{15\ \%}$/Epoxy has been applied for the heat dissipation of LED chips, which exhibits better ability than that of commercial silicone sheet. More importantly, the 3D BNNS/CNTs$_{15\ \%}$/Epoxy composite can maintain a high electrical resistivity above 10^{10} Ω m. Furthermore, it exhibits high elastic modulus of 1.0 GPa and tensile stress of 35 MPa. Therefore, this work may open up new avenues for the development of advanced electric insulating material with excellent thermal and mechanical performance for electronic device.

Declaration of competing interest

The authors declare that they have no known competing financial interests or personal relationships that could have appeared to influence

the work reported in this paper.

Acknowledgments

We gratefully acknowledge the financial supports from the National Natural Science Foundation of China (Nos. 21808240, 21776308, and 21908245), Science Foundation of China University of Petroleum, Beijing (Nos. 2462018YJRC009).

Appendix A. Supplementary data

Supplementary data related to this article can be found at https://doi.org/10.1016/j.compositesb.2021.109168.

References

[1] Chen H, Ginzburg VV, Yang J, Yang Y, Liu W, Huang Y, Du L, Chen B. Thermal conductivity of polymer-based composites: fundamentals and applications. Prog Polym Sci 2016;59:41–85.
[2] Moore AL, Shi L. Emerging challenges and materials for thermal management of electronics. Mater Today 2014;17:163–74.
[3] Zeng X, Sun J, Yao Y, Sun R, Xu JB, Wong CP. A combination of boron nitride nanotubes and cellulose nanofibers for the preparation of a nanocomposite with high thermal conductivity. ACS Nano 2017;11:5167–78.
[4] Fang H, Bai SL, Wong CP. "White graphene"-hexagonal boron nitride based polymeric composites and their application in thermal management. Compos. Commun. 2016;2:19–24.
[5] Yu C, Gong W, Tian W, Zhang Q, Xu Y, Lin Z, Hu M, Fan X, Yao Y. Hot-pressing induced alignment of boron nitride in polyurethane for composite films with thermal conductivity over 50 W m^{-1} K^{-1}. Compos Sci Technol 2018;160:199–207.
[6] Kuang Z, Chen Y, Lu Y, Liu L, Hu S, Wen S, Mao Y, Zhang L. Fabrication of highly oriented hexagonal boron nitride nanosheet/elastomer nanocomposites with high thermal conductivity. Small 2015;11:1655–9.
[7] Zhang X, Zhang J, Xia L, Wang J, Li C, Xu F, Zhang X, Wu H, Guo S. Achieving high-efficiency and robust 3D thermally conductive while electrically insulating hybrid filler network with high orientation and ordered distribution. Chem Eng J 2018;334:247–56.
[8] Yu C, Zhang J, Li Z, Tian W, Wang L, Luo J, Li Q, Fan X, Yao Y. Enhanced through-plane thermal conductivity of boron nitride/epoxy composites. Compos. Part. A-Appl. Sci. Manuf. 2017;98:25–31.
[9] Li Q, Tian X, Chen Z, Wu J, Li Y, Li Y. Synergistic effect of size distribution on the electrical and thermal conductivities of graphene-based paper. J Mater Sci 2018;53:10261–9.
[10] Chen J, Huang X, Zhu Y, Jiang P. Cellulose nanofiber supported 3D interconnected BN nanosheets for epoxy nanocomposites with ultrahigh thermal management capability. Adv Funct Mater 2017;27:1604754.
[11] Zeng X, Yao Y, Gong Z, Wang F, Sun R, Xu J, Wong CP. Ice-templated assembly strategy to construct 3D boron nitride nanosheet networks in polymer composites for thermal conductivity improvement. Small 2015;11:6205–13.
[12] Zhang X, Zhang J, Xia L, Li C, Wang J, Xu F, Zhang X, Wu H, Guo S. Simple and consecutive melt extrusion method to fabricate thermally conductive composites with highly oriented boron nitrides. ACS Appl Mater Interfaces 2017;9:22977–84.
[13] Kim P, Shi L, Majumdar A, McEuen PL. Thermal transport measurements of individual multiwalled nanotubes. Phys Rev Lett 2001;87:215502.
[14] Luo W, Wang Y, Hitz E, Lin Y, Yang B, Hu L. Solution processed boron nitride nanosheets: synthesis, assemblies and emerging applications. Adv Funct Mater 2017;27:1701450.
[15] Zhang X, Zhang J, Li C, Wang J, Xia L, Xu F, Zhang X, Wu H, Guo S. Endowing the high efficiency thermally conductive and electrically insulating composites with excellent antistatic property through selectively multilayered distribution of diverse functional fillers. Chem Eng J 2017;328:609–18.
[16] Yin J, Li J, Hang Y, Yu J, Tai G, Li X, Zhang Z, Guo W. Boron nitride nanostructures: fabrication, functionalization and applications. Small 2016;12:2942–68.
[17] Wu K, Fang J, Ma J, Huang R, Chai S, Chen F, Fu Q. Achieving a collapsible, strong, and highly thermally conductive film based on oriented functionalized boron nitride nanosheets and cellulose nanofiber. ACS Appl Mater Interfaces 2017;9:30035–45.
[18] Xie A, Wang Y, Jiang P, Li S, Huang X. Nondestructive functionalization of carbon nanotubes by combining mussel-inspired chemistry and RAFT polymerization: towards high dielectric nanocomposites with improved thermal management capability. Compos Sci Technol 2018;154:154–64.
[19] Hu J, Huang Y, Yao Y, Pan G, Sun J, Zeng X, Sun R, Xu JB, Song B, Wong CP. Polymer composite with improved thermal conductivity by constructing a hierarchically ordered three-dimensional interconnected network of BN. ACS Appl Mater Interfaces 2017;9:13544–53.
[20] Z. Wang, G. Meng, L. Wang, L. Tian, S. Chen, G. Wu, B. Kong, Y. Cheng, Simultaneously enhanced dielectric properties and through-plane thermal conductivity of epoxy composites with alumina and boron nitride nanosheets[J]. Sci Rep 11(1) 2021 1-202111.
[21] Loeblein M, Tay RY, Tsang SH, Ng WB, Teo EHT. Configurable three-dimensional boron nitride-carbon architecture and its tunable electronic behavior with stable thermal performances. Small 2014;10:2992–9.
[22] Zhou W, Zhang Y, Wang J, Li H, Xu W, Li B, Chen L, Wang Q. Lightweight porous polystyrene with high thermal conductivity by constructing 3D interconnected network of boron nitride nanosheets. ACS Appl Mater Interfaces 2020;12:46767–78.
[23] Liu B, Li Y, Fei T, Han S, Xia C, Shan Z, Jiang J. Highly thermally conductive polystyrene/polypropylene/boron nitride composites with 3D segregated structure prepared by solution-mixing and hot-pressing method. Chem Eng J 2020;385:123829.
[24] Tian X, Li Y, Chen Z, Li Q, Hou L, Wu J, Tang Y, Li Y. Shear-assisted production of few-layer boron nitride nanosheets by supercritical CO_2 exfoliation and its use for thermally conductive epoxy composites. Sci Rep 2017;7:1–9.
[25] Fan Z, Yan J, Zhi L, Zhang Q, Wei T, Feng J, Zhang M, Qian W, Wei F. A three-dimensional carbon nanotube/graphene sandwich and its application as electrode in supercapacitors. Adv Mater 2010;22:3723–8.
[26] Yan W, Zhang Y, Sun H, Liu S, Chi Z, Chen X, Xu J. Polyimide nanocomposites with boron nitride-coated multi-walled carbon nanotubes for enhanced thermal conductivity and electrical insulation. J Mater Chem A 2014;2:20958–65.
[27] Jiang J, Liu J, Zhou W, Zhu J, Huang X, Qi X, Zhang H, Yu T. CNT/Ni hybrid nanostructured arrays: synthesis and application as high-performance electrode materials for pseudocapacitors. Energy Environ Sci 2011;4:5000–7.
[28] Huang J, Zhu N, Yang T, Zhang T, Wu P, Dang Z. Nickel oxide and carbon nanotube composite (NiO/CNT) as a novel cathode non-precious metal catalyst in microbial fuel cells. Biosens Bioelectron 2015;72:332–9.
[29] Song Y, Li B, Yang S, Ding G, Zhang C, Xie X. Ultralight boron nitride aerogels via template-assisted chemical vapor deposition. Sci Rep 2015;5:1–9.
[30] Li LH, Cervenka J, Watanabe K, Taniguchi T, Chen Y. Strong oxidation resistance of atomically thin boron nitride nanosheets. ACS Nano 2014;8:1457–62.
[31] Liu Z, Shen D, Yu J, Dai W, Li C, Du S, Jiang N, Li H, Lin C. Exceptionally high thermal and electrical conductivity of three-dimensional graphene-foam-based polymer composites. RSC Adv 2016;6:22364–9.
[32] Liu Z, Chen Y, Li Y, Dai W, Yan Q, Alam FE, Du S, Wang Z, Nishimura K, Jiang NJN. Graphene foam-embedded epoxy composites with significant thermal conductivity enhancement. Nanoscale 2019;11:17600–6.
[33] Kargar F, Barani Z, Salgado R, Debnath B, Lewis JS, Aytan E, Lake RK, Balandin AA. Thermal percolation threshold and thermal properties of composites with high loading of graphene and boron nitride fillers. ACS Appl Mater Interfaces 2018;10:37555–65.
[34] Guo Y, Lyu Z, Yang X, Lu Y, Ruan K, Wu Y, Kong J, Gu J. Enhanced thermal conductivities and decreased thermal resistances of functionalized boron nitride/polyimide composites. Compos B Eng 2019;164:732–9.
[35] Chen C, Xue Y, Li Z, Wen Y, Li X, Wu F, Li X, Shi D, Xue Z, Xie X. Construction of 3D boron nitride nanosheets/silver networks in epoxy-based composites with high thermal conductivity via in-situ sintering of silver nanoparticles. Chem Eng J 2019;369:1150–60.
[36] M, Li M, Wang X, Hou Z, Zhan H, Wang H, Fu CT, Lin L, Fu N, Jiang J, Yu. Highly thermal conductive and electrical insulating polymer composites with boron nitride. Compos B Eng 2020;184:107746.
[37] Li Y, Tian X, Yang W, Li Q, Hou L, Zhu Z, Tang Y, Wang M, Zhang B, Pan T. Dielectric composite reinforced by in-situ growth of carbon nanotubes on boron nitride nanosheets with high thermal conductivity and mechanical strength. Chem Eng J 2019;358:718–24.
[38] Jiang F, Cui X, Song N, Shi L, Ding P. Synergistic effect of functionalized graphene/boron nitride on the thermal conductivity of polystyrene composites. Compos. Commun. 2020;20:100350.
[39] Jiang F, Cui S, Rungnim C, Song N, Shi L, Ding P. Control of a dual-cross-linked boron nitride framework and the optimized design of the thermal conductive network for its thermoresponsive polymeric composites. Chem Mater 2019;31:7686–95.
[40] Lewis JS, Barani Z, Magana AS, Kargar F, Balandin A. Thermal and electrical conductivity control in hybrid composites with graphene and boron nitride fillers. Mater Res Express 2019;6:085325.
[41] Wang ZG, Liu W, Liu YH, Ren Y, Li YP, Zhou L, Xu JZ, Lei J, Li Z. Highly thermal conductive, anisotropically heat-transferred, mechanically flexible composite film by assembly of boron nitride nanosheets for thermal management. Compos B Eng 2020;180:107569.
[42] Hong H, Jung YH, Lee JS, Jeong C, Kim JU, Lee S, Ryu H, Kim H, Ma Z, Kim T. Anisotropic thermal conductive composite by the guided assembly of boron nitride nanosheets for flexible and stretchable electronics. Adv Funct Mater 2019;29:1902575.
[43] Ren J, Li Q, Yan L, Jia L, Huang X, Zhao L, Ran Q, Fu M. Enhanced thermal conductivity of epoxy composites by introducing graphene@boron nitride nanosheets hybrid nanoparticles. Mater Des 2020;191:108663.
[44] Shang Y, Yang G, Su F, Feng Y, Ji Y, Liu D, Yin R, Liu C, Shen C. Multilayer polyethylene/hexagonal boron nitride composites showing high neutron shielding efficiency and thermal conductivity. Compos. Commun. 2020;19:147–53.
[45] Moradi S, Román F, Calventus Y, Hutchinson J. Remarkable thermal conductivity of epoxy composites filled with boron nitride and cured under pressure. Polymers 2021;13:955.

[46] Han G, Zhao X, Feng Y, Ma J, Zhou K, Shi Y, Liu C, Xie X. Highly flame-retardant epoxy-based thermal conductive composites with functionalized boron nitride nanosheets exfoliated by one-step ball milling. Chem Eng J 2021;407:127099.
[47] Liang Y, Zhang B, Liu Z, Liu M. Electroless deposition surface engineering of boron nitride sheets for enhanced thermal conductivity and decreased interfacial thermal resistance of epoxy composites. Int J Heat Mass Tran 2021;174:121306.
[48] Kim JM, Jung DW, Kim LS, Kim M, Jeong S, Lee S, Chang SJ, Cho JY, Kim SH, Park J, Choi K, Yi G, Nam K, Lee G. Continuously thermal conductive pathway of bidisperse boron nitride fillers in epoxy composite for highly efficient heat dissipation. Mater. Today. Commun. 2021;27:102230.